Journal of Sound and Vibration (2001) **248**(2), 351–370
doi:10.1006/jsvi.2001.3757, available online at http://www.idealibrary.com on IDEAL®

AUTO-REGRESSIVE SVD ALGORITHMS AND CUTTING STATE IDENTIFICATION

B. S. Berger, J. A. Manzari, D. K. Anand and C. Belai

Department of Mechanical Engineering, University of Maryland, College Park, MD 20742, *U.S.A.*

(*Received* 28 *February* 2000, *and in final form* 27 *April* 2001)

Functions of the singular values of matrices of third order cumulants associated with the TOR, CTOM and OARM algorithms for parametric bispectral estimation are shown to identify cutting states associated with the orthogonal cutting of stiff cylinders. Test functions and experimentally measured cutting tool accelerations are examined. Algorithms for auto-regressive approximations utilizing cumulants of arbitrary order are shown to characterize cubically phase-coupled test functions.

1. INTRODUCTION

A review of cutting vibration research is presented in reference [1]. Previous cutting models and methods of chatter detection are given in references [2–13].

Recently developed signal processing methodologies including wavelets, neural networks and information-theoretic functionals have been applied to the analysis and control of cutting dynamics. Wavelet transforms were employed in reference [14] to study non-regenerative thread and slot cutting processes. Time–frequency plots based on Gaussian wavelet transforms were used to detect and characterize non-stationary phenomena such as built up edge breakage. Wavelet analysis indicates that the non-regenerative cutting process is probably quadratically non-linear [15]. Cutting states, associated with the orthogonal cutting of stiff metal cylinders, were identified in reference [16] through an analysis of the ratios of the mean absolute deviations of details of the biorthogonal 6,8 wavelet decompositions of cutting force measurements. The kurtosis of detail d_3 was shown to identify transitions to chatter.

In reference [17], two back propagation neural networks, one for frequency estimation, the other for sine wave identification, were trained on numerically generated sine and triangular waves. Chatter vibrations were assumed to have a harmonic shape, exponential growth of amplitude and a frequency similar to the lowest natural frequency of the structure. The trained neural network was able to detect the onset of chatter for the turning of long slender bars.

Discrimination between chatter and non-chatter cutting states was achieved in reference [18] through an analysis utilizing the coarse-grained entropy rate. A significant decrease of the entropy rate was shown to indicate the onset of chatter.

The identification of cutting states, associated with the orthogonal cutting of stiff steel cylinders, was realized in reference [19] through an analysis of the behavior of the singular values of a Toeplitz matrix, **R**, of third order cumulants of tool acceleration measurements. The **R** matrix determined the coefficients in an auto-regressive (AR) approximation of the bispectrum based on the third order recursion method (TOR) [20]. A bispectral and

0022-460X/01/470351 + 20 $35.00/0

bicoherency analysis of the cutting tool acceleration measurements showed that the cutting process is quadratically phase coupled [15]. Reference [19] shows the ratio of the sum of the largest pair of singular values of **R** to the sum of the second largest pair, the *R*-ratio, differentiated between light cutting, medium cutting, pre-chatter and chatter states.

A study of parametric methods for the detection of phase coupling through approximation of the bicoherency and bispectrum was given in references [21, 22] in which the performances of the TOR, CTOM constrained third order mean [21] and OARM, optimized AR method [23] algorithms were compared. For the examples presented, it was found that CTOM was superior to TOR in the resolution of peaks in the bispectrum, while for reduced data sets OARM was superior to TOR. TOR, CTOM and OARM were shown to resolve peaks in the bispectrum more accurately than the conventional method.

In the following, the coefficient matrix for the P unknown coefficients in the AR approximation of the given time series is denoted by **R**, equation (14), **Q**, equation (25), $\mathbf{r}_2$, equation (30) for the TOR, CTOM and OARM algorithms respectively. Q- and r_2-ratios associated with **Q** and $\mathbf{r}_2$ are defined identically to the R-ratio associated with the **R** matrix. Three quadratically phase-coupled trigonometric functions $f_i(t)$, equations (32)–(34), constructed in reference [19] approximate R, Q and r_2-ratios associated with measured tool acceleration for chatter, light and medium orthogonal cutting. Although, for a given $f_i(t)$, singular values of **R**, **Q** and $\mathbf{r}_2$ matrices differ by orders of magnitude, the associated R, Q and r_2-ratios are nearly identical when evaluated over an extended data set of 15 records of 1024 samples each. The R, Q and r_2-ratios approach 2 for $f_1(t)$, the chatter state. The R and Q-ratios are nearly identical for all three $f_i(t)$. The r_2-ratio as a function of matrix size or maxlag is similar in behavior to the R and Q-ratios. It is shown that the ratios evaluated for an appropriate matrix size or value of maxlag characterize the $f_i(t)$. The ratios, evaluated over reduced data sets, remain capable of characterizing the functions $f_i(t)$. The R, Q and r_2-ratios are found for the extended data set to which the colored Gaussian noise of variance = 1·0 had been added. The effect of the noise on the ratios is shown to be slight. The ratios characterized the functions $f_i(t)$ for the reduced data set with added colored Gaussian noise of variance = 0·5. The R, Q and r_2-ratios were found for an experimentally measured set of cutting tool accelerations associated with the chatter state. The ratios are in good agreement for maxlag > 50. Although TOR, CTOM and OARM all characterize the functions $f_i(t)$ and the chatter data, the robustness and computational efficiency of TOR recommends it.

The elements of matrices **R**, **Q** and $\mathbf{r}_2$ are functions of third order cumulants. Singular values of the **C** and **S** matrices associated with AR approximations by cumulants of arbitrary order are studied as a function of matrix size or maxlag. It is shown that the associated C and S ratios characterize cubically phase-coupled test functions. The R, Q, and r_2-ratios have a potential application in the control of orthogonal cutting in which quadratic phase coupling is present. The C and S ratios may be useful in the control of cutting systems in which cubic or higher order phase coupling is present.

2. THIRD ORDER RECURSION

The following definitions and theorems [22, 24] provide a background in higher order spectral theory for a subsequent application. Let $m_n(\tau_1, \tau_2, \ldots, \tau_{n-1}) \equiv$ the nth order moment of a real nth order stationary random process $X(k)$, $k = 0, \pm 1, \pm 2, \ldots$. Then,

$$m_n(\tau_1, \tau_2, \ldots, \tau_{n-1}) \equiv E[X(k)X(k+\tau_1)\cdots X(k+\tau_{n-1})]. \tag{1}$$

E is the expected value, which may be estimated by

$$m_n(\tau_1, \tau_2, \ldots, \tau_{n-1}) = (1/2m + 1) \sum_{k=-m}^{+m} X(k)X(k+\tau_1)\cdots X(k+\tau_{n-1}), \tag{2}$$

where $m \to +\infty$. For a set of random variables $\{x_1, x_2, \ldots, x_n\}$ the joint cumulants $Cum[x_1, x_2, \ldots, x_n]$ of order n are given by

$$Cum[x_1, x_2, \ldots, x_n] = \sum_p (-1)^{P-1}(P-1)!E\left\{\prod_{i\in s_1} x_i\right\}E\left\{\prod_{i\in s_2} x_i\right\}\cdots E\left\{\prod_{i\in s_P} x_i\right\}, \tag{3}$$

where summations extend over all partitions $(s_1, s_2, \ldots, s_p)$ $p = 1, 2, \ldots, n$ of the set of integers $(1, 2, \ldots, n)$. Let

$$c_n^x(\tau_1, \tau_2, \ldots, \tau_{n-1}) \equiv Cum[X(k), X(k+\tau_1), \ldots, X(k+\tau_{n-1})]. \tag{4}$$

Then equations (1), (3) and (4) imply that

$$c_1^x = m_1^x, \qquad c_2^x(\tau_1) = m_2^x(\tau_1) - (m_1^x)^2, \tag{5, 6}$$

$$c_3^{(x)}(\tau_1, \tau_2) = m_3^x(\tau_1, \tau_2) - m_1^x[m_2^x(\tau_1) + m_2^x(\tau_2) + m_2^x(\tau_2 - \tau_1)] + 2(m_1^x)^3. \tag{7}$$

These expressions take a simpler form if $m_1^x = 0$. In the subsequent computations the mean, m_1^x is always subtracted from the time series. Then,

$$\begin{aligned} c_4^x(\tau_1, \tau_2, \tau_3) = m_4^x(\tau_1, \tau_2, \tau_3) &- m_2^x(\tau_1)m_2^x(\tau_3 - \tau_2) \\ &- m_2^x(\tau_2)m_2^x(\tau_3 - \tau_1) - m_2^x(\tau_3)m_2^x(\tau_2 - \tau_1). \end{aligned} \tag{8}$$

In general, the cumulant $c_n^x(\tau_1, \tau_2, \ldots, \tau_{n-1})$, equation (4), is symmetric for any permutation of its arguments [24]. Third order cumulants satisfy further symmetries [21], including

$$c_3^x(\tau_1, \tau_2) = c_3^x(-\tau_1, \tau_2 - \tau_1) \tag{9}$$

and

$$c_3^x(\tau_1, \tau_2) = c_3^x(\tau_1 - \tau_2, -\tau_2). \tag{10}$$

The $(n-1)$th order spectrum of $X(k)$, $C_n(\tau_1, \tau_2, \ldots, \tau_{n-1})$, is defined by

$$\begin{aligned} C_n(\omega_1, \omega_2, \ldots, \omega_{n-1}) = &\sum_{\tau_1=-\infty}^{+\infty}\sum_{\tau_2=-\infty}^{+\infty}\cdots\sum_{\tau_{n-1}=-\infty}^{+\infty} c_n(\tau_1, \tau_2, \ldots, \tau_{n-1}) \\ &\times \exp[-\mathrm{j}(\omega_1\tau_1 + \omega_2\tau_2 + \cdots + \omega_{n-1}\tau_{n-1})]. \end{aligned} \tag{11}$$

Consider an AR estimation of the bispectrum, $C_3(\omega_1, \omega_2)$, equation (11) [21, 25]. A Pth order AR process is described by

$$X(n) + \sum_{i=1}^{P} a(i)X(n-i) = W(n), \tag{12}$$

where it is assumed that $W(k)$ is non-Gaussian, $E(W(k)) = 0$, $E(W^3(k)) = \beta$. Multiplying through equation (12) by $X(n-k)X(n-\ell)$, summing and noting equation (2) gives

$$c_3^x(-k,-\ell) + \sum_{i=1}^{P} a(i) c_3^x(i-k, i-\ell) = \beta\delta(k,\ell), \tag{13}$$

the third order recursion equation, where $k \geqslant 0$, $\ell \geqslant 0$. $\delta(0,0) = 1$ and $\delta(k,\ell) = 0$ for all other positive values of k and ℓ. Three algorithms TOR, CTOM and OARM, have been proposed for the determination of the AR coefficients $a(i)$ [20, 21, 23]. The singular values of matrices associated with these algorithms provide a basis for the identification of the cutting state.

3. TOR

The TOR algorithm, for the determination of the AR coefficient $a(i)$, follows from the third order recursion equation (13), letting $k = \ell$, $k = 0, \ldots, P$. This yields $P+1$ equations for the $P+1$ unknowns $a(i)$ and β; $P+1 \equiv$ maxlag. In matrix notation,

$$\mathbf{Ra} = \mathbf{b}, \tag{14}$$

where

$$\mathbf{R} = \begin{bmatrix} g(0,0) & g(1,1) & \cdots & g(P,P) \\ g(-1,-1) & g(0,0) & \cdots & g(P-1,P-1) \\ \vdots & & & \vdots \\ g(-P,-P) & g(-P+1,-P+1) & \cdots & g(0,0) \end{bmatrix}, \tag{15}$$

and where $g(i,j) \equiv c_3^x(i,j)$, $\mathbf{a} = [1, a(1), \ldots, a(P)]^{\mathrm{T}}$ and $\mathbf{b} \equiv [\beta, 0, \ldots, 0]^{\mathrm{T}}$. $\mathbf{R}$ is, in general, a non-symmetric Toeplitz matrix. Sufficient conditions for the representation in equation (14) to exist are given in reference [22]. The bispectrum corresponding to equation (13) is given by references [20, 22]

$$C_3^x(\omega_1, \omega_2) = \beta H(\omega_1) H(\omega_2) H^*(\omega_1 + \omega_2), \tag{16}$$

where

$$H(\omega) = 1 \Big/ \left(1 + \sum_{n=1}^{P} a(i) \exp(-\mathrm{j}\omega n)\right) \tag{17}$$

and $H^*(\omega) \equiv$ complex conjugate of $H(\omega)$. An estimate of the $\mathbf{R}$ matrix, equation (15), for a data set $X(i)$, $i = 1, \ldots, N$, may be formed [20] as follows:

(1) Segment the data set into κ records of M samples each. $X^i(k)$, $k = 1, 2, \ldots, M$, are data points associated with the ith record.
(2) Compute $c_{3,i}^x(m,n)$ for the ith record as

$$c_{3,i}^x(m,n) = (1/M) \sum_{\ell=a}^{b} X^{(i)}(\ell) X^{(i)}(\ell+m) X^{(i)}(\ell+n). \tag{18}$$

where $i = 1, 2, \ldots, \kappa$, $a \equiv \max(1, 1-m, 1-n)$ and $b \equiv \min(M, M-m, M-n)$.

(3) Average $c^x_{3,i}(m, n)$ over all κ records,

$$\hat{c}_3(m, n) = (1/K) \sum_{i=1}^{\kappa} c^x_{3,i}(m, n) \tag{19}$$

to yield the estimate $\hat{c}_3(m, n)$, from an estimated **R** matrix by replacing $c^x_3(m, n)$ by $\hat{c}_3(m, n)$ in equation (15). Values of M and K, equation (18), which reduce the total duration of the required data set and algorithmic execution time were estimated by a direct parametric search; Figures 4 and 5. Functions of the singular values of equation (15) are subsequently used in cutting state identification.

4. CTOM

The constrained third order mean (CTOM) [21], provides an alternative set of linear algebraic equations for the determination of AR coefficients, a_i. Define

$$\hat{q}_m(k, i) \equiv X(m - i)X^2(m - k), \tag{20}$$

where $i = 1, \ldots, P$. It follows from equations (1), (2), and (7) that

$$E\{\hat{q}_m(k, i)\} = c^x_3(i - k, i - k). \tag{21}$$

Equation (13) may then be expressed in terms of $\hat{q}_m(k, i)$ as

$$E\{\hat{C}(m, k)\} = 0 \tag{22}$$

with

$$\hat{C}(m, k) \equiv \hat{q}_m(k, 0) + \sum_{i=1}^{P} a(i)\hat{q}_m(k, i). \tag{23}$$

$N - P$ samples of $\hat{C}(m, k)$ may be found for $m = P + 1, P + 2, \ldots, N$; $k = 1, \ldots, P$. Equation (22) is satisfied by equating the sample mean to zero:

$$\frac{1}{N - P} \sum_{m=P+1}^{N} \hat{C}(m, k) = 0 \tag{24}$$

for $k = 1, \ldots, P$. Expressing equation (24) in matrix form gives

$$\mathbf{Q}\ \mathbf{a} = \mathbf{b}, \tag{25}$$

where $\mathbf{Q} = [\hat{q}_{ij}]$, $i, j = 1, \ldots, P$, $a = [a(1), \ldots, a(P)]^{\mathrm{T}}$, $b = [\hat{q}_{i0}]^{\mathrm{T}}$ and

$$\hat{q}_{ij} = \sum_{m=P+1}^{N} \hat{q}_m(i, j). \tag{26}$$

If the time series is divided into κ records of equal length, then $\hat{q}_{ij}$ may be approximated by the value of $\hat{q}_m(i, j)$ for the nth record, $\hat{q}^{(n)}_m(i, j)$ averaged over κ records. Then, equation (26) becomes

$$\hat{q}_{ij} = \frac{1}{\kappa} \sum_{n=1}^{\kappa} \sum_{m=P+1}^{M} \hat{q}^{(n)}_m(i, j). \tag{27}$$

CTOM is asymptotically equivalent to TOR for a given AR order [21] and gives consistent AR parameter estimates for processes satisfying equation (12).

5. OARM

The optimized AR method [23] follows from equation (13) with $k = 0, 1, \ldots, s$ and $\ell = 0, 1, \ldots, s$. Equation (13) becomes

$$\mathbf{r}\,\mathbf{a} = \mathbf{b}, \tag{28}$$

where

$$\mathbf{r} = \begin{bmatrix} (0,0) & (-1,-1) & \cdots & (-s,-s) \\ (0,1) & (-1,0) & \cdots & (-s,-s+1) \\ \vdots & \vdots & & \vdots \\ (0,s) & (-1,s-1) & \cdots & (-s,0) \\ (1,0) & (0,-1) & \cdots & (-s+1,-s) \\ \vdots & \vdots & & \vdots \\ (s,s) & (s-1,s-1) & \cdots & (0,0) \end{bmatrix}, \tag{29}$$

$\mathbf{a} = a[1, a(1), \ldots, a(P)]^{\mathrm{T}}$, $\mathbf{b} = [\beta, 0, \ldots, 0]^{\mathrm{T}}$, $(i,j) = c_3^x(i,j)$ and $\mathbf{r}$ is $(P+1)^2 \times (P+1)$ with $s = P$. A least-squares solution of equation (29) is $\mathbf{a} = (\mathbf{r}^{\mathrm{T}}\mathbf{r})^{-1}\mathbf{r}^{\mathrm{T}}\mathbf{b}$ which implies that

$$\mathbf{r}_2\mathbf{a} = \mathbf{r}^{\mathrm{T}}\mathbf{b}, \tag{30}$$

where $\mathbf{r}_2 \equiv \mathbf{r}^{\mathrm{T}}\mathbf{r}$. TOR is a special case of OARM form with $k = \ell$. The elements of the $\mathbf{r}$ matrix, $c_3^x(i,j)$, may be estimated by averaging over κ records of M samples each; equation (19).

6. SINGULAR-VALUE DECOMPOSITION

Properties of singular values are discussed and applied to phase-coupled test functions, chosen to model chatter, light and medium orthogonal cutting. If $\mathbf{A}$ is a real $m \times n$ matrix, then there exists orthogonal matrices $\mathbf{U} \in R^{m \times n}$ and $\mathbf{V} \in R^{m \times n}$ such that

$$\mathbf{U}^{\mathrm{T}}\mathbf{A}\mathbf{V} = \mathrm{diag}(\sigma_1, \ldots, \sigma_q) \in R^{m \times n}, \tag{31}$$

where $q = \min(m, n)$, $\sigma_1 \geqslant \sigma_2 \geqslant \cdots \sigma_q \geqslant 0$ are the singular values and $R^{m \times n}$ denotes a real $m \times n$ matrix. If $\sigma_1 \geqslant \cdots \geqslant \sigma_r \geqslant \sigma_{r+1} = \cdots = \sigma_q = 0$, then rank $(A) = r$; references [26, 27].

The following three quadratically phase-coupled trigonometric functions:

$$\begin{aligned} f_1(t) = {} & \cos(2\pi\,100t + \theta_1) + \cos(2\pi 100t + \theta_2) \\ & + 0{\cdot}2\cos(2\pi\,200t + \theta_1 + \theta_2), \end{aligned} \tag{32}$$

$$\begin{aligned} f_2(t) = {} & 0{\cdot}9\cos(2\pi\,90t + \theta_1) + 1{\cdot}0\cos(2\pi 100t + \theta_2) \\ & + 0{\cdot}2\cos(2\pi\,190t + \theta_1 + \theta_2), \end{aligned} \tag{33}$$

$$f_3(t) = \cos(2\pi 90t + \theta_1) + \cos(2\pi 100t + \theta_2) + \cos(2\pi 190t + \theta_1 + \theta_2) + \cos(2\pi 100t + \theta_3) + \cos(2\pi 110t + \theta_4) + 0{\cdot}5\cos(2\pi 210t + \theta_3 + \theta_4) \quad (34)$$

were constructed to approximate the R, Q and r_2-ratios associated with measured tool accelerations for chatter, light and medium orthogonal cutting, respectively; reference [19]. The phases θ_i are mutually independent and uniformly distributed over $[0, 2\pi]$.

7. STATE CHARACTERIZATION

The singular values of an $m \times n$ matrix may be ordered as $\sigma_1 \geqslant \sigma_2 \geqslant \sigma_3 \geqslant \sigma_4 \geqslant \cdots \geqslant \sigma_q \geqslant 0$, equation (31). Denote the ratio $(\sigma_1 + \sigma_2)/(\sigma_3 + \sigma_4)$ for a matrix $\mathbf{A}$ as the A-ratio. The R, Q and r_2-ratios associated with the $\mathbf{R}$, $\mathbf{Q}$ and $\mathbf{r}_2$ matrices, equations (15), (25), (27) and (30), respectively, have been found for each of the test functions, f_i, equations (32)–(34) besides a set of measured tool accelerations associated with chatter. The R, Q and r_2-ratios are shown to discriminate between the test functions and to be consistent for the chatter data. Although the magnitudes of the singular values of the $\mathbf{R}$, $\mathbf{Q}$ and $\mathbf{r}_2$ matrices vary widely, the corresponding R, Q and r_2-ratios are for the most part nearly identical.

Three data sets were constructed consisting of test functions $f_i(t)$, $i = 1, 2, 3$ sampled at 1024 Hz and arranged in 15 records of 1024 values each. The singular values of the $\mathbf{R}$, $\mathbf{Q}$ and $\mathbf{r}_2$ matrices and the R, Q and r_2-ratios were found by averaging the appropriate function, equations (19), (27), (30), over the15 records associated with each $f_i(t)$.

The function $f_1(t)$ is self-phase coupled at a frequency of 100 Hz. In the experimental data studied, cutting states closer to chatter always exhibited power spectral components in the neighborhood of 100 and 200 Hz and a single peak in the bispectrum in the neighborhood of (100 Hz, 100 Hz), [19]. For $f_1(t)$, the means of the dominant pairs of singular values of $\mathbf{R}$ are seen to be linear functions of maxlag in Figure 1(a). The corresponding R-ratio converges to a value of 2 for maxlag > 60, Figure 1(b). Similar behavior is exhibited by the singular values of $\mathbf{Q}$. Although the magnitudes of the singular values of $\mathbf{Q}$ differ from those of $\mathbf{R}$ by a factor of 10^3 the Q-ratio oscillates with a small amplitude about a value of 2, Figure 2(a) and 2(b). For $f_1(t)$, the singular values of $\mathbf{r}_2$ versus maxlag differ from those of $\mathbf{R}$ and $\mathbf{Q}$, Figure 3(a). However, the Q-ratio converges to a value of 2 for maxlag > 80, Figure 3(b). It is evident that the number of pairs of singular values equals the number of different frequency components in $f_1(t)$.

Function $f_2(t)$, equation (33), exhibits phase coupling of 90 and 100 Hz components. The coupling of side bands to the central 100 Hz frequency component has been observed in the experimental data associated with light and medium cutting. The R-ratios for $f_2(t)$ and light cutting data are similar [19]. Singular values of $\mathbf{R}$ and $\mathbf{Q}$ matrices and the R and Q-ratios as functions of maxlag, Figures 1(c) and 2(c), 1(d) and 2(d) are identical. For maxlag $= 100$ the R and Q-ratios, equal 1 and are bounded between 1 and 1·2 for maxlag > 100. The r_2-ratio is similar to the R and Q-ratios, reaching a minimum of 1·2 for maxlag $= 100$ and is bounded between 1·2 and 1·25 for maxlag > 100, Figure 3(c) and 3(d). The number of pairs of singular values, 3, is seen to equal the number of different frequency components in $f_2(t)$.

Functions $f_3(t)$, equation (34), is the sum of a phase-coupled component at 100 and 110 Hz and a phase coupling of 90 and 100 Hz components. The R-ratios for $f_3(t)$ and medium cutting data are similar [19]. Singular values of $\mathbf{R}$ and $\mathbf{Q}$ matrices and R and Q-ratios, Figures 1(e) and 2(e), 1(f) and 2(f) are nearly identical. For the R and Q-ratios,

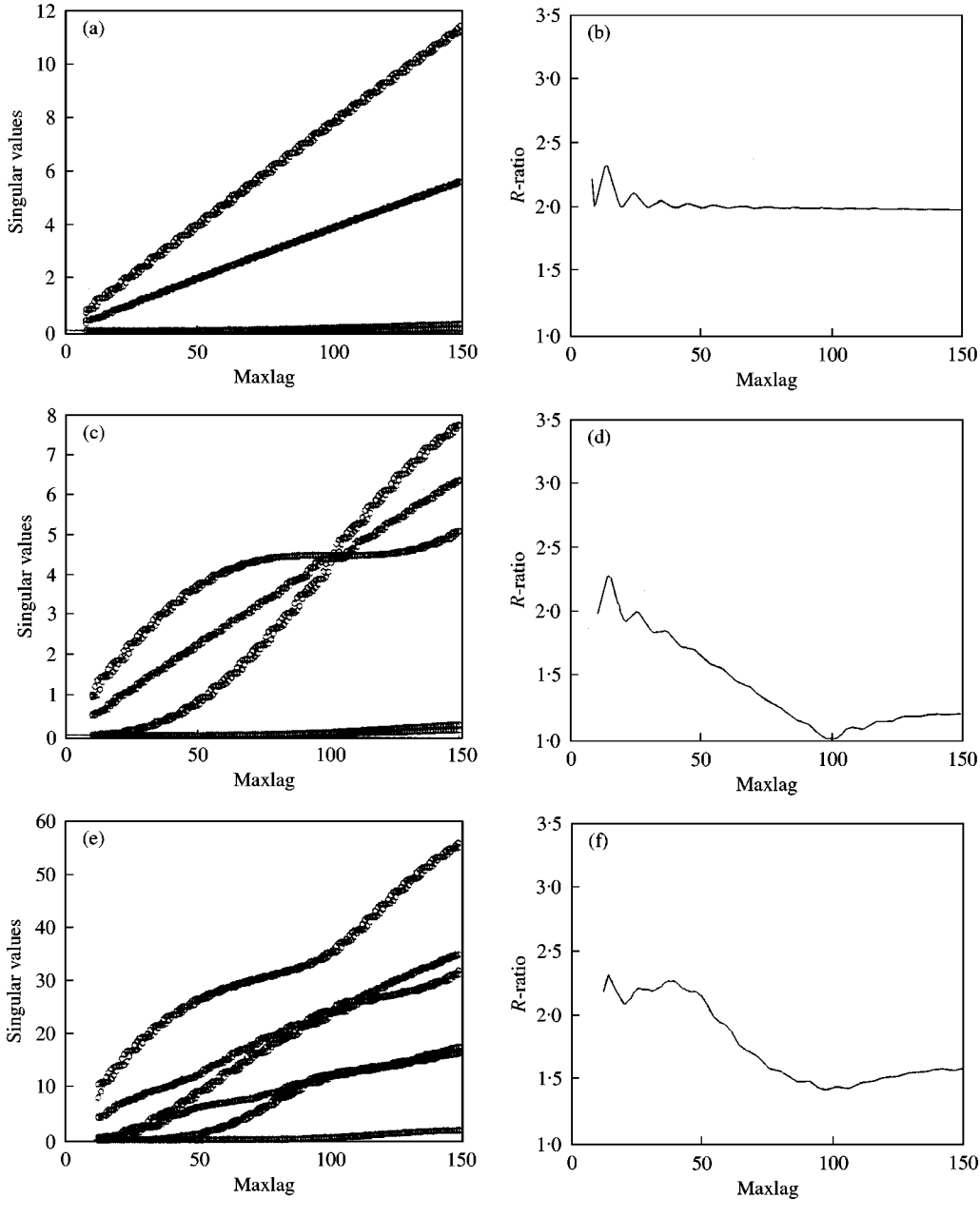

Figure 1. $f_i(t)$ with n samp = 1024, f samp = 1024 Hz, n record = 15. For $i = 1$: (a) singular values and (b) R-ratio versus maxlag; for $i = 2$: (c) singular values and (d) R-ratio versus maxlag; for $i = 3$: (e) singular values and (f) R-ratio versus maxlag.

respectively, at maxlag = 100, minimums of 1·46 and 1·52 are attained and $1{\cdot}46 < R < 1{\cdot}62$, $1{\cdot}52 < Q < 1{\cdot}63$ for maxlag > 100. The r_2-ratio is similar to the R and Q-ratios reaching a minimum of 1·28 at maxlag = 100 and is bounded between 1·28 and 1·50 for maxlag > 100, Figure 3(e) and 3(f). Five pairs of singular values are evident which correspond to the five frequency components present in $f_3(t)$.

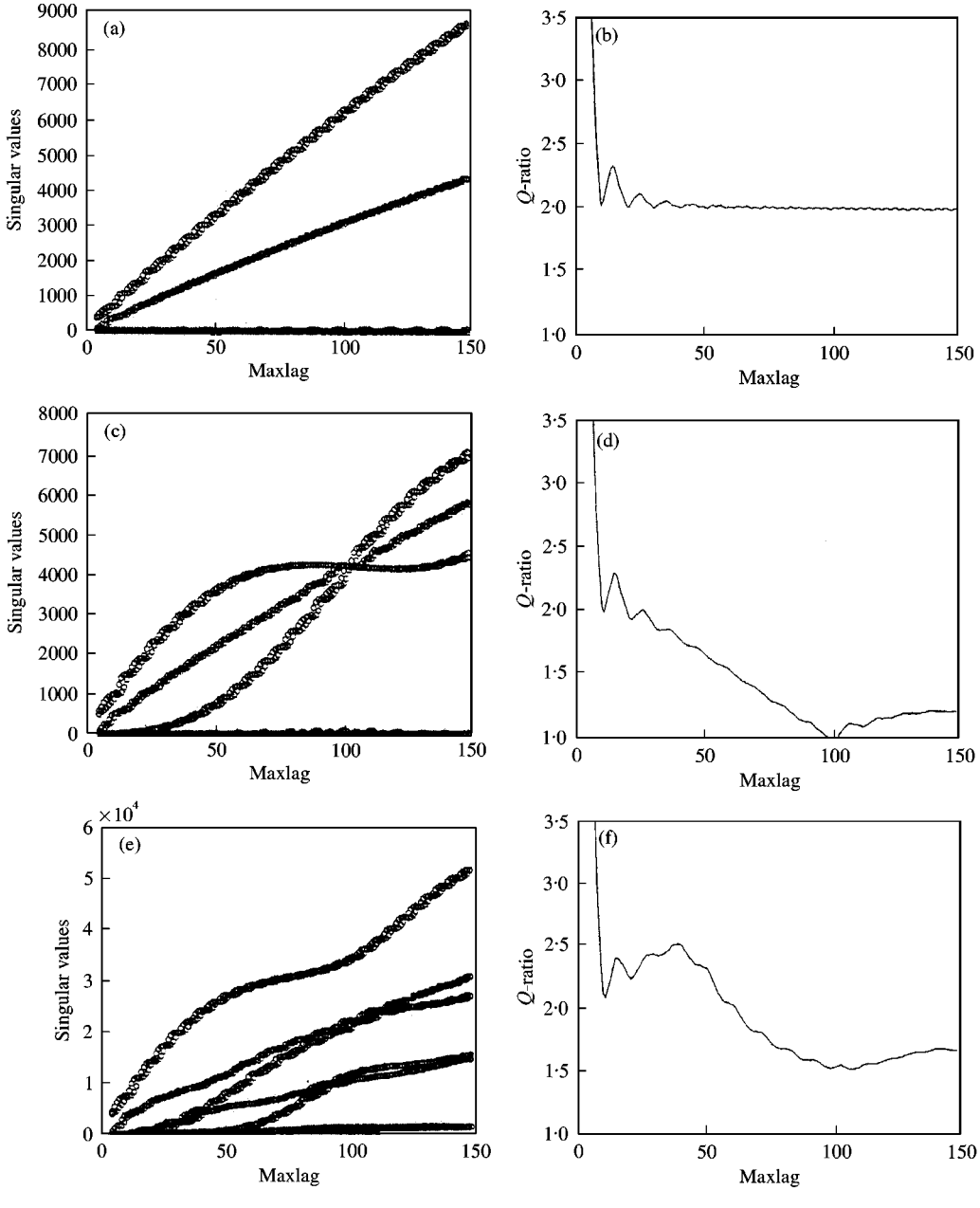

Figure 2. $f_i(t)$ with n samp = 1024, f samp = 1024 Hz, n record = 15. For $i = 1$: (a) singular values and (b) Q-ratio versus maxlag; for $i = 2$: (c) singular values and (d) Q-ratio versus maxlag; for $i = 3$: (e) singular values and (f) Q-ratio versus maxlag.

Rapid identification of the current cutting state is essential for the on-line control of the cutting process. To this end, parametric studies were carried out in which sampling rates, record size and number were varied. Three data sets were formed consisting of $f_i(t)$, $i = 1, 2, 3$ sampled at 1024 Hz and arranged in three records of 256 samples each for a time series 0·75 s in length. The singular values of the **R**, **Q** and $\mathbf{r}_2$ matrices and the R, Q and

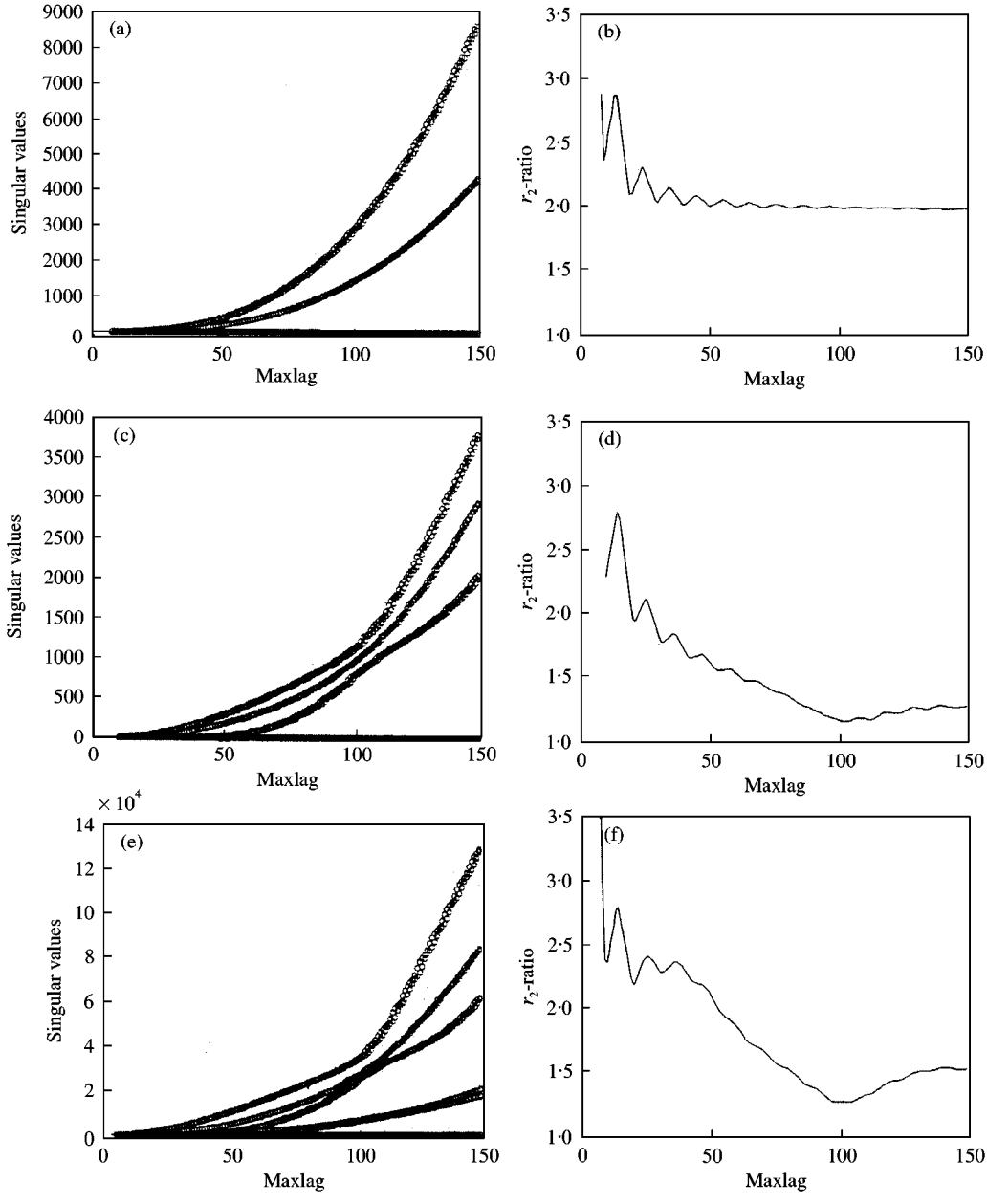

Figure 3. $f_i(t)$ with n samp = 1024, f samp = 1024 Hz, n record = 15. For $i = 1$: (a) singular values and (b) r_2-ratio versus maxlag; for $i = 2$: (c) singular values and (d) r_2-ratio versus maxlag; for $i = 3$: (e) singular values and (f) r_2-ratio versus maxlag.

r_2-ratios were computed by averaging the appropriate functions over the three records associated with each $f_i(t)$. Figures 4 and 5 show the results of the computation. Comparison of Figure 4(a) and 4(b) for $f_1(t)$ with Figure 1(a) and 1(b), singular values of **R** matrices and the R-ratios for 15 records of 1024 samples each sampled at 1024 Hz, shows the figures to be identical. Figure 4(c) and 4(d), for $f_2(t)$, is nearly identical to Figure 1(c) and 1(d). The minimum of the R-ratio for $f_3(t)$, Figure 4(f), at maxlag = 100 is 1·56, while for the more

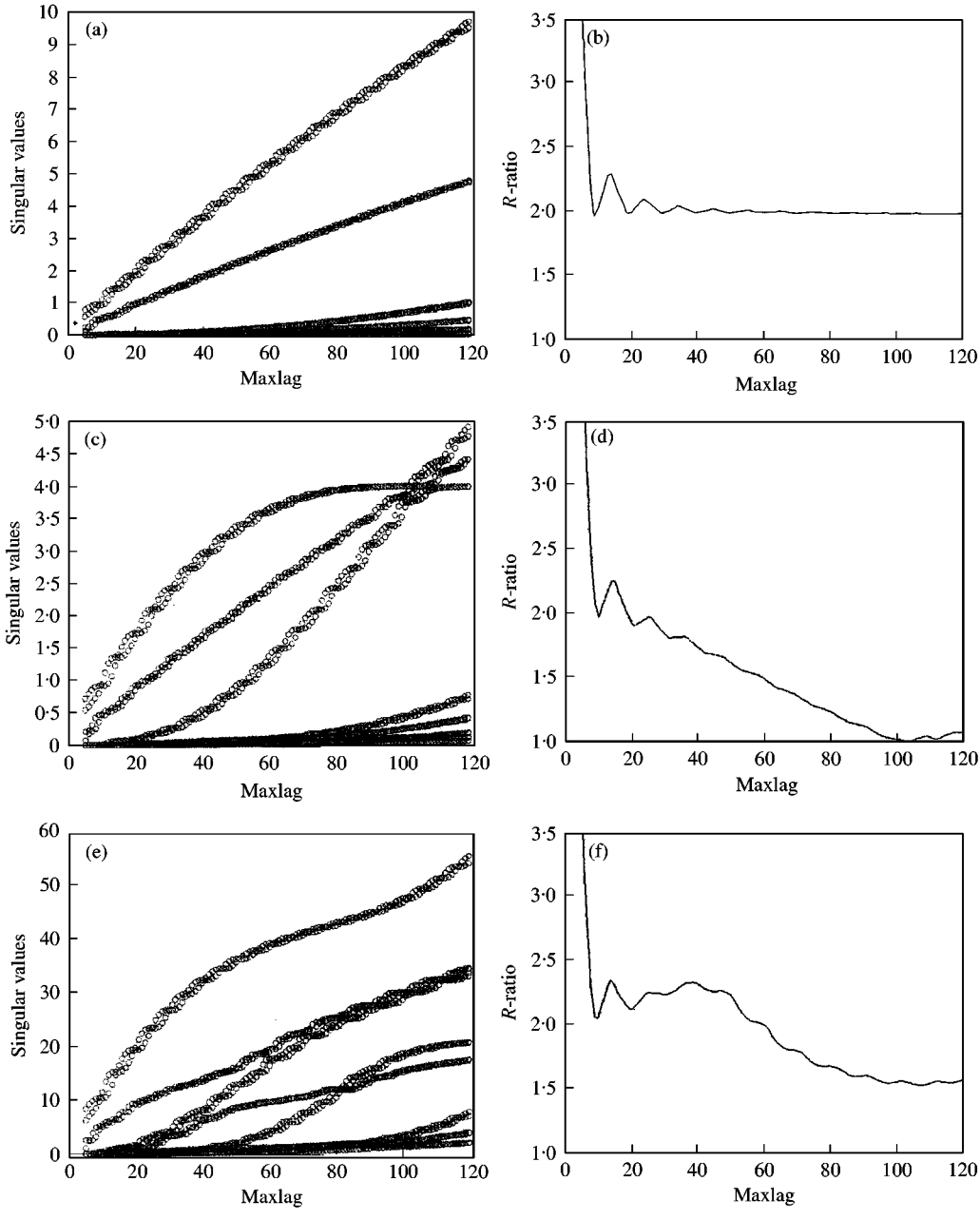

Figure 4. $f_i(t)$ with n samp $= 256$, f samp $= 1024$ Hz, n record $= 3$. For $i = 1$: (a) singular values and (b) R-ratio versus maxlag; for $i = 2$: (c) singular values and (d) R-ratio versus maxlag; for $i = 3$: (e) singular values and (f) R-ratio versus maxlag.

accurate result shown in Figure 1(f) the minimum is 1·46. Figure 5 displays the singular values of **Q** matrices and the Q-ratios for f_i, $i = 1, 2, 3$ based on the reduced data set of three records each of 256 samples. A comparison with Figure 3 shows the superposition of oscillations on the more accurate result. However, the approximation is sufficiently accurate to characterize the functions f_i.

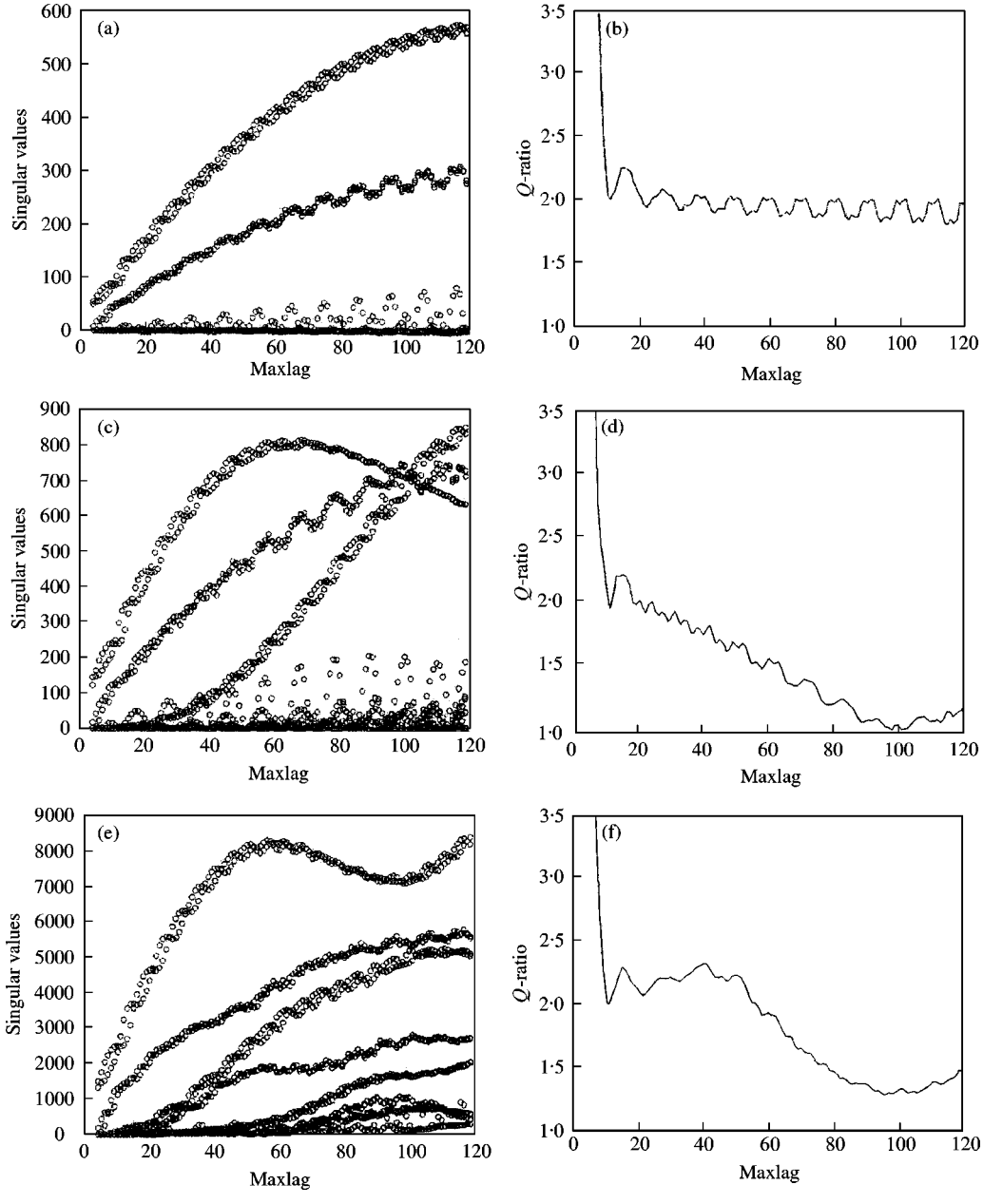

Figure 5. $f_i(t)$ with n samp $= 256$, f samp $= 1024$ Hz, n record $= 3$. For $i = 1$: (a) singular values and (b) Q-ratio versus maxlag; for $i = 2$: (c) singular values and (d) Q-ratio versus maxlag; for $i = 3$: (e) singular values and (f) Q-ratio versus maxlag.

For $k \geqslant 3$ the cumulants $c_k(\tau_1, \tau_2, \ldots, \tau_{k-1})$, equations (2), and (7), are known to be insensitive to added Gaussian noise for sufficiently large values of m in equation (2) [22, 24]. The magnitude of error, for a given $f_i(t)$, in the numerical computation of singular values of the **R**, **Q**, and $\mathbf{r}_2$ matrices occasioned by additive Gaussian noise is shown to be a function of the magnitude of the noise variance and m. Gaussian noise with a variance $= 1$ was added

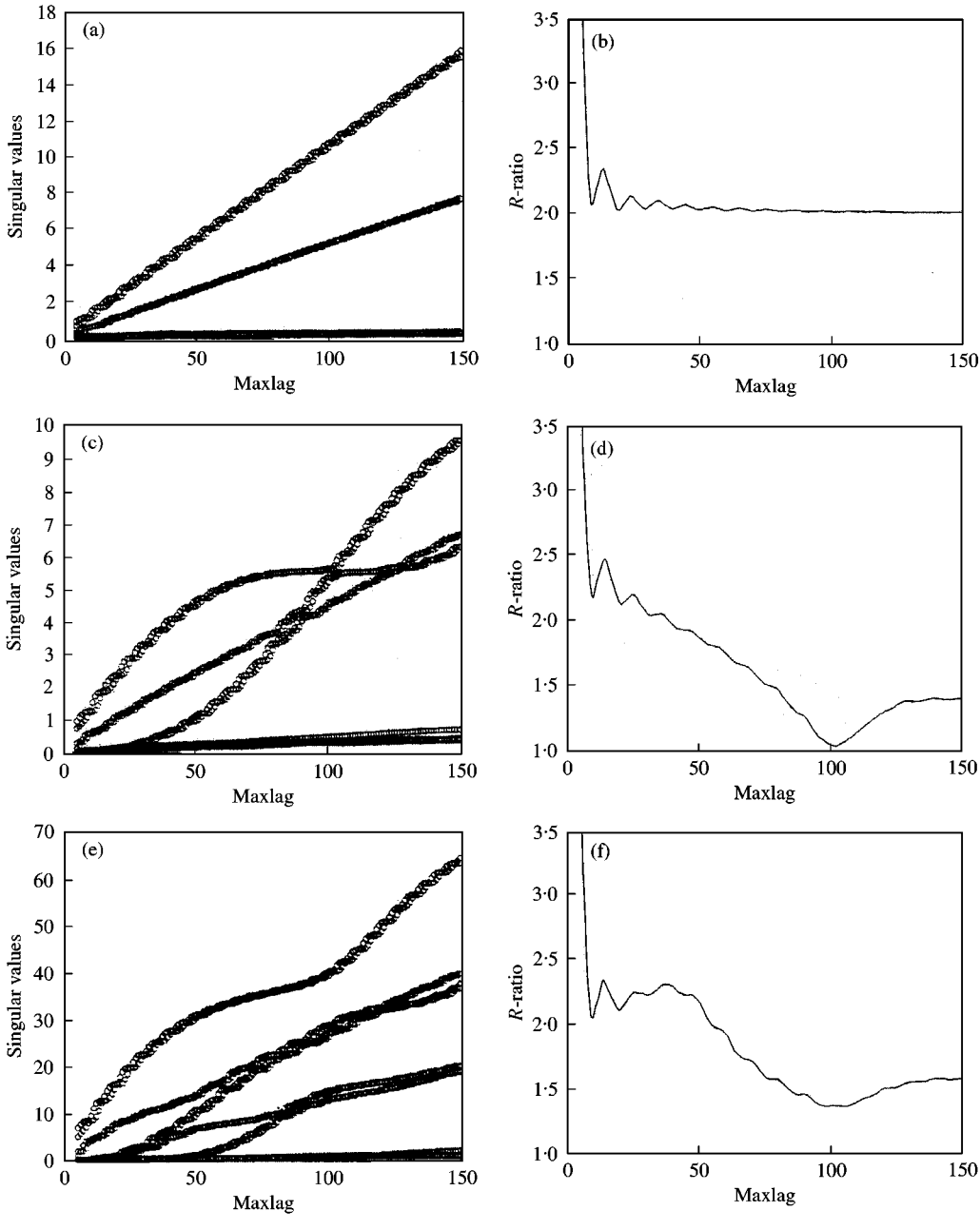

Figure 6. $f_i(t)$ + Gaussian noise of variance = 1 with n samp = 1024, f samp = 1024 Hz, n record = 15. For $i = 1$: (a) singular values and (b) R-ratio versus maxlag; for $i = 2$: (c) singular values and (d) R-ratio versus maxlag; for $i = 3$: (e) singular values and (f) R-ratio versus maxlag.

to the $f_i(t)$ functions. Three data sets were formed for $f_i(t)$, $i = 1, 2, 3$ sampled at 1024 Hz and arranged in 15 records of 1024 samples each. The corresponding singular values of the **R** matrix, equation (15) and the R-ratios are shown in Figure 6. Figure 6(a) and 6(b) for $f_1(t)$ plus noise is identical to Figure 1(a) and 1(b) for the noiseless case. The qualitative behavior of the R-ratio for $f_2(t)$ plus noise, Figure 6(d), is similar to the noiseless case, Figure 1(d),

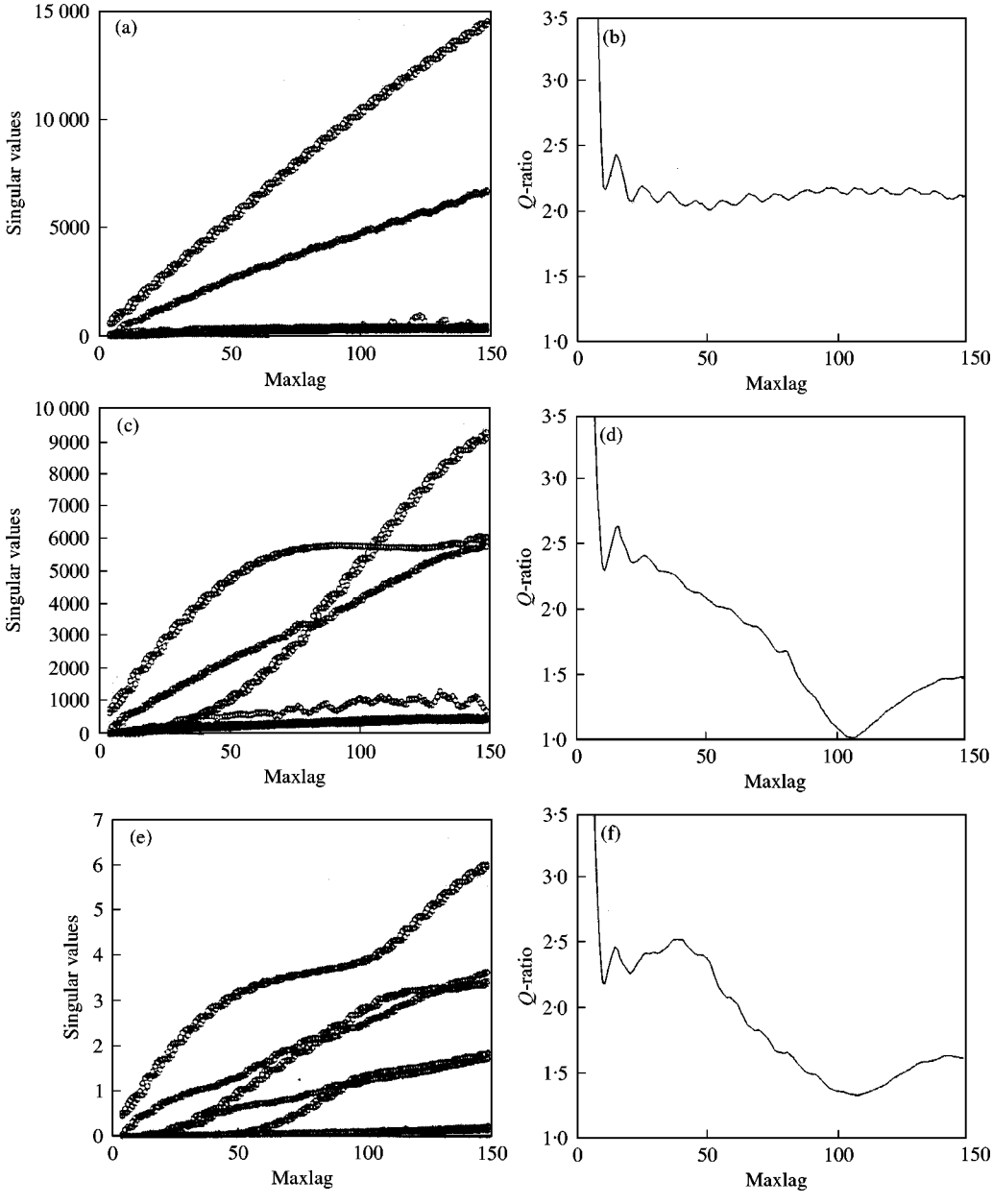

Figure 7. $f_i(t)$ + Gaussian noise of variance = 1 with n samp = 1024, f samp = 1024 Hz, n record = 15. For $i = 1$: (a) singular values and (b) Q-ratio versus maxlag; for $i = 2$: (c) singular values and (d) Q-ratio versus maxlag; for $i = 3$: (e) singular values and (f) Q-ratio versus maxlag.

decreasing to a minimum of 1 for maxlag = 100. Figure 6(e) and 6(f) for $f_3(t)$ plus noise is nearly identical to Figure 1(e) and 1(f) for the noiseless case.

As in the case of the R-ratio, the Q-ratio, equation (25), associated with CTOM, gives ratios for $f_i(t)$ plus noise, Figure 7, which are qualitatively similar to those found for the noiseless case, Figure 2. Similar calculations of the R and Q-ratios based on the reduced data set with added Gaussian noise of variance = 0·50 displayed qualitative similarities

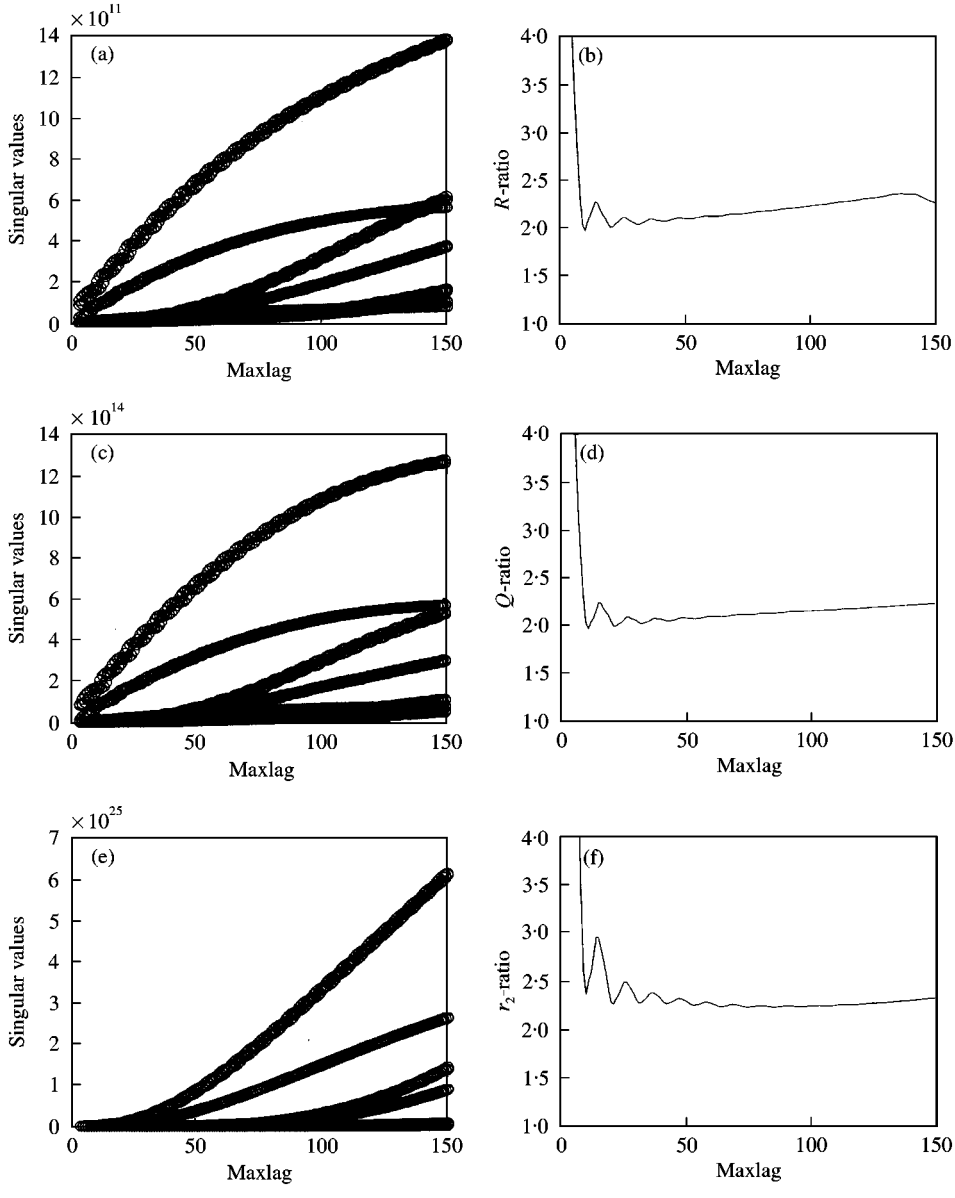

Figure 8. Set 1: (a) **R** singular values versus maxlag; (b) R-ratio versus maxlag; (c) **Q** singular values versus maxlag; (d) Q-ratio versus maxlag; (e) $\mathbf{r}_2$ singular values versus maxlag; (f) r_2-ratio versus maxlag.

between the noiseless and noisy cases. For both the extended and reduced noisy data sets, the R and Q-ratios identified the test functions, $f_i(t)$.

The TOR, CTOM and OARM algorithms were applied to the analysis of experimentally measured tool acceleration chatter data, set 1, for which depth of cut = 2·8 mm, feed rate = 0·007 in/rev, surface speed = 90 m/min, sampling rate = 1024 Hz and duration = 1·0 s. The corresponding R, Q and r_2-ratios, shown in Figure 8, are in good agreement for maxlag > 50. Previous studies of the measured tool acceleration chatter data [19] have shown that an R-ratio $\geqslant 2$ is associated with the chatter state.

8. AR APPROXIMATION BY CUMULANTS OF ARBITRARY ORDER

The previous discussion has been limited to Toeplitz matrices of third order cumulants, $c_3(\tau_1, \tau_2)$, associated with AR approximation. For systems with cubic or higher order non-linearities, algorithms based on third order cumulants would fail. Two algorithms for the determination of ARMA parameters [28–30] provide matrices of cumulants of arbitrary order suitable for singular-value analysis. Consider the causal ARMA model

$$\sum_{j=0}^{P} a(j)\, y(i-j) = \sum_{j=0}^{q} b(j) w(i-j), \tag{35}$$

where $y(i)$ is the output and the input $w(i)$ is stationary, zero mean, i.i.d., non-Gaussian with kth order cumulant γ_k^w. Since $w(i)$ is i.i.d. its kth order cumulant may be expressed as

$$c_k^w(i_1, i_2, \ldots, i_{k-1}) = \gamma_k^w \delta(i_1, i_2, \ldots, i_{k-1}). \tag{36}$$

where $\delta(i_1, i_2, \ldots, i_{k-1})$ denotes the Kronecker delta function. The kth order output cumulants are then given by [28, 29]

$$c_k^y(i_1, i_2, \ldots, i_{k-1}) = \gamma_k^w \sum_{i=0}^{+\infty} h(i) h(i+i_1) \ldots h(i+i_{k-1}), \tag{37}$$

where $h(m) \equiv$ ARMA response function. Let

$$c_k^y(m, n) \equiv c_k^y(m, n, 0, \ldots, 0) \tag{38}$$

for $k \geqslant 3$. Substituting equation (38) into equation (37) gives

$$c_k^y(m, n) = \gamma_k^w \sum_{i=0}^{\infty} h(i)^{k-2} h(i+m) h(i+n). \tag{39}$$

It can be shown [28] that

$$h(i+m) = -\sum_{j=1}^{p} a(j) h(i+m-j) + b(i+m). \tag{40}$$

Combining equations (39) and (40) gives

$$c_k^y(m, n) + \sum_{j=1}^{p} a(j) c_k^y(m-j, n) = \begin{cases} Q, & m \leqslant q, \\ 0, & m > q, \end{cases} \tag{41}$$

where $Q = \gamma_k^w \sum_{i=0}^{\infty} h(i)^{k-2} b(i+m) h(i+n)$. Letting $n = q-p, \ldots, q$, $m = q+1, \ldots, q+p$ in equation (41) gives $p(p+1)$ equations for the coefficients $a(i)$, $i = 1, \ldots, p$ [28]:

$$\mathbf{C}\,\mathbf{a} = \mathbf{b}, \tag{42}$$

where

$$\mathbf{C} = \begin{bmatrix} (q+1-p, q-p) & \cdots & (q, q-p) \\ \vdots & \vdots & \vdots \\ (q+1-p, q) & \cdots & (q, q) \\ & \vdots & \\ (q, q-p) & \cdots & (q+p-1, q-p) \\ \vdots & \vdots & \vdots \\ (q, q) & \cdots & (q+p-1, q) \end{bmatrix}, \tag{43}$$

$\mathbf{a} = [a(p), a(p-1), \ldots, a(1)]^{\mathrm{T}}$ and $\mathbf{b} = -[(q+1, q-p), \ldots, (q+1, q), \ldots, (q+p, q-p), \ldots, (q+p, q)]^{\mathrm{T}}$. $c_k^y(m, n) \equiv (m, n)$. Taking the product of the $p(p+1) \times p$ matrix $\mathbf{C}$ with $\mathbf{C}^{\mathrm{T}}$ gives

$$\mathbf{C}_{sq}\mathbf{a} = \mathbf{C}^{\mathrm{T}}\mathbf{b}, \tag{44}$$

where $\mathbf{C}_{sq} \equiv \mathbf{C}^{\mathrm{T}}\mathbf{C}$ is $p \times p$. Assumptions inherent in the deviation of equation (42) are given in references [28, 30]. The singular values of $\mathbf{C}_{sq}$ will be examined subsequently.

A second algorithm for ARMA parameter estimation [30] follows the derivation of reference [28], equations (35)–(41). In reference [30], equation (41) is written in the form

$$\sum_{j=0}^{P} a(j) c_k^y(m-j, n) = 0 \tag{45}$$

for $m > q$, where $n = q-p, \ldots, q$ and $m = q+1, \ldots, q+p+M$, $M \geqslant 0$. Expressing equation (45) as $\mathbf{S}\,\mathbf{a} = 0$, $\mathbf{S}_{sq}$ is defined as

$$\mathbf{S}_{sq} = \mathbf{S}^{\mathrm{T}}\mathbf{S}. \tag{46}$$

For a proper choice of p, q and M, the AR parameters, $a(j)$, are identified by equation (45), [30]. In practice, the true ARMA orders, p and q are not usually known. Assuming that these parameters are overestimated by $P \geqslant p$ and $Q \geqslant q$, letting $n = -P, \ldots, Q$ and $m = Q+1, \ldots, Q+P$ will include a sufficient amount of data in providing a robust estimate of the singular values of the $\mathbf{S}$ matrix. The elements of the $\mathbf{C}$ and $\mathbf{S}$ matrices may be estimated by averaging over κ records of M samples each; equation (19).

9. CUBIC PHASE COUPLING

Relationships between cubically phase-coupled trigonometric functions and the singular values of the $\mathbf{C}_{sq}$ and $\mathbf{S}_{sq}$ matrices were considered through a study of functions $g_i(t)$, $i = 1, 2$:

$$g_1(t) = 0{\cdot}25\cos(2\pi 100t + \theta_1) + 0{\cdot}25\cos(2\pi 100t + \theta_2) + 1{\cdot}0\cos(2\pi 130t + \theta_3) + 0{\cdot}86\cos(2\pi 330t + \theta_1 + \theta_2 + \theta_3), \tag{47}$$

$$g_2(t) = 1{\cdot}0\cos(2\pi 100t + \theta_1) + 1{\cdot}0\cos(2\pi 110t + \theta_2) + 1{\cdot}0\cos(2\pi 160t + \theta_3) + 0{\cdot}15\cos(2\pi 370t + \theta_1 + \theta_2 + \theta_3), \tag{48}$$

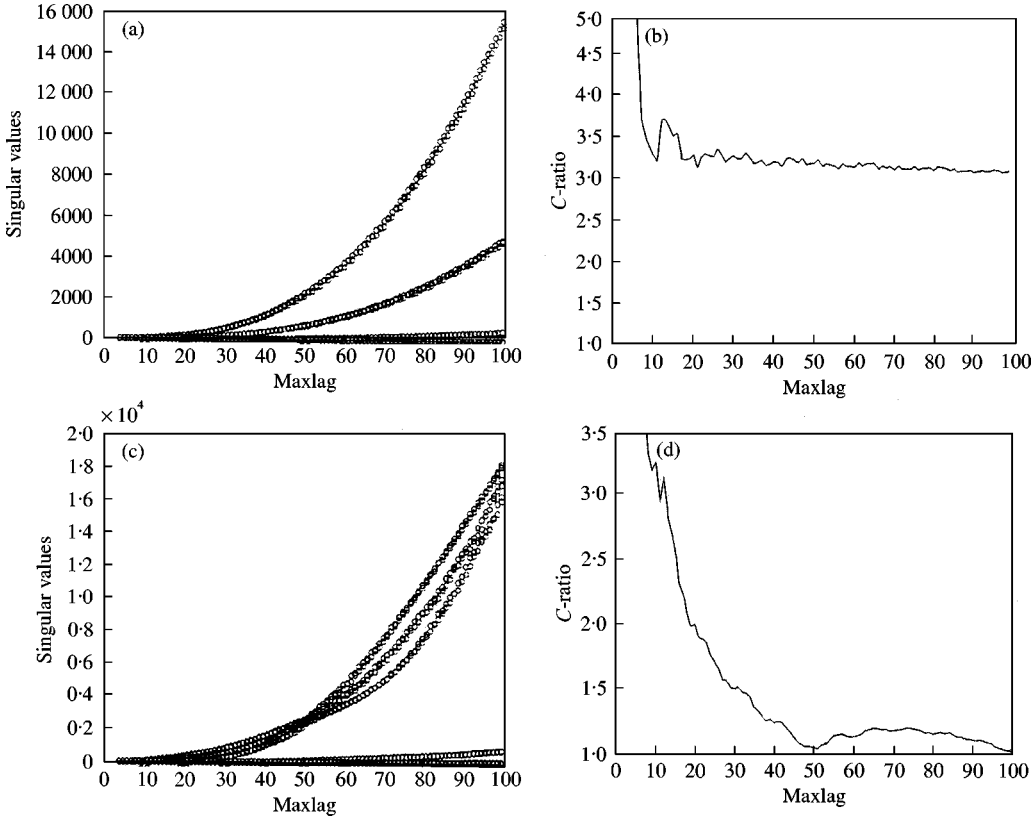

Figure 9. $g_i(t)$ with n samp = 512, f samp = 512, n record = 15. For $i = 1$: (a) singular values and (b) C-ratio versus maxlag; for $i = 2$: (c) singular values and (d) C-ratio versus maxlag.

where the phases θ_i are mutually independent and uniformly distributed over $[0, 2\pi]$. Two data sets were constructed consisting of cubically phase-coupled test functions $g_i(t)$, $i = 1, 2$; equations (47) and (48), sampled at 512 Hz and arranged in 15 records of 512 values each. The singular values of the **C** and $\mathbf{S}_{sq}$ matrices equations (43) and (46), and the *C and* S_{sq} ratios were found by averaging the appropriate function over the 15 records associated with each $g_i(t)$.

$g_1(t)$ is the sum of two components at 100 Hz together with components at 130 and 330 Hz. Three pairs of singular values of the **C** matrix are evident in Figure 9(a). The C-ratio is seen to approach a value of $\simeq 3{\cdot}2$ in Figure 9(b) for maxlag = 100. The singular values and C-ratio verses maxlag for $g_i(t)$ are qualitatively similar to those for the quadratically phase-coupled function $f_1(t)$; equation (32), Figure 3(a, b).

The modulated function $g_2(t)$, equation (48), is the sum of four components at 100, 110, 160 and 370 Hz. Four pairs of singular values of the **C** matrix appear in Figure 9(c). The C-ratio approaches a value of 1·0 at intervals of 50 maxlags. Three of the largest pairs of singular values have a common value of maxlag = 50 which corresponds to approximately 10 Hz, the modulation frequency, with a sampling rate of 512 Hz. A similarity is evident between Figures 9(c, d) and 3(c, d) for the quadratically coupled $f_2(t)$; equation (33). An analysis of $g_i(t)$ based on the $\mathbf{S}_{sq}$ matrix gave the results identical to those shown in Figure 9.

10. CONCLUSIONS

In references [21, 22], the algorithms CTOM and OARM were shown to resolve the peaks in the bispectrum of a set of phase-coupled test functions more accurately than the TOR algorithm. The present study demonstrates that for a set of phase-coupled test functions modelling the orthogonal cutting of stiff metal cylinders [19] and an example of experimentally measured cutting tool accelerations, ratios of singular values associated with TOR, CTOM and OARM identify the test functions and cutting state. However, the relative computational simplicity and speed of TOR together with its invariance in the presence of high levels of Gaussian noise indicate greater effectiveness than CTOM and OARM in the on-line control of cutting states.

The above algorithms detect quadratic or second order phase coupling but not third or higher order coupling. In the present study, ratios of singular values associated with matrices of fourth order cumulants were shown to identify test functions with cubic phase coupling.

ACKNOWLEDGMENTS

The authors acknowledge the support of the National Science Foundation through GER-9354956. The encouragement of H. L. Russell of the University of Maryland, College Park, P. Grootenhuis and D. J. Ewins of the Imperial College of Science, Technology and Medicine, London, is very much appreciated. M. Rokni read the manuscript, making a number of important suggestions. The assistance of T. Miller in the presentation of the manuscript has been invaluable.

REFERENCES

1. J. TLUSTY 1979 *CIRP Annals* **27**, 583–589. Analysis of the state of research in cutting dynamics.
2. I. KOENIGSBERGER and J. TLUSTY 1971 *Structure of Machine Tools*. New York: Pergamon Press.
3. M. WECK 1985 *Handbook of Machine Tools*, Vol. 4. New York: John Wiley.
4. H. R. TAYLOR 1977 *Proceedings of the Institute of Mechanical Engineers* **191**, 257–270. A comparison of methods for measuring the frequency response of mechanical structures with particular reference to machine tools.
5. K. J. KIM, E. F. EMAN and S. M. WU 1984 *International Journal of Machine Tool Design and Research* **27**, 161–170. Identification of natural frequencies and damping ratios of machine tool structures by the dynamic data system approach.
6. M. E. MERCHANT 1945 *Journal of Applied Physics* **16**, 267–275. Mechanics of metal cutting process I.
7. D. W. WU 1989 *Transactions of the American Society of Mechanical Engineers, Journal of Engineering for Industry* **11**, 37–47. A new approach to formulating the transfer function for dynamic cutting processes.
8. J. S. LIN and C. I. WENG 1990 *International Journal of Machine Tools and Manufacturing* **30**, 53–64. A nonlinear model of cutting.
9. T. Y. AHN, K. F. EMAN and S. M. WU 1985 *Transaction of the American Society of Mechanical Engineers, Journal of Engineering for Industry* **107**, 91–94. Cutting dynamics identification by dynamic data system modeling approach.
10. J. PETERS, P. VANDERCK and H. VAN BRUSSEL 1971 *CIRP Annals* **20**, 129–136. The measurement of the dynamic cutting coefficient.
11. T. DELIO, J. TLUSTY and S. SMITH 1992 *American Society of Mechanical Engineers, Journal of Engineering for Industry* **114**, 146–157. Use of audio signals for chatter detection and control.
12. I. GRABEC 1986 *Physics Letters* **117**, 384–386. Chaos generated by the cutting process.
13. I. GRABEC 1988 *International Journal of Machine Tools and Manufacturing* **28**, 275–280. Chaotic dynamics of the cutting process.

14. M. K. KHRAISHEN, C. PEZESHKI and A. E. BAYOUMI 1995 *Journal of Sound and Vibration* **180**, 67–87. Time series based analysis for primary chatter in metal cutting.
15. B. S. BERGER, I. MINIS, K. DENG, Y. S. CHEN, A. CHAVALI and M. ROKNI 1996 *Journal of Sound and Vibration* **191**, 986–992. Phase coupling in orthogonal cutting.
16. B. S. BERGER, I. MINIS, J. HARLEY, M. ROKNI and M. PAPADOPOULOS 1998 *Journal of Sound and Vibration* **213**, 813–827. Wavelet based cutting state identification.
17. I. N. TANSEL, A. WAGIMAN and T. TZIRANIR 1991 *International Journal of Machine Tools and Manufacturing* **31**, 539–552. Recognition of chatter with neural networks.
18. J. GRADISEK, E. GOVEKAR and I. GRABEC 1998 *Journal of Sound and Vibration* **214**, 941–952. Using coarse-grained entropy rate to detect chatter in cutting.
19. B. S. BERGER, I. MINIS, M. ROKNI M. PAPADOPOULOS, K. DENG and A. CHAVALLI 1997 *Journal of Sound and Vibration* **200**, 15–29. Cutting state identification.
20. M. R. RAGHUVEER and C. L. NIKIAS 1985 *IEEE Transactions on Acoustics, Speech and Signal Processing* **ASSP-33**, 1213–1230. Bispectrum estimation: a parametric approach.
21. M. R. RAGHUVEER and C. L. NIKIAS 1986 *Signal Processing* **10**, 35–48. Bispectrum estimation via AR modeling.
22. C. L. NIKIAS and A. P. PETROPULU 1993 *Higher-order Spectra Analysis*. Englewood Cliffs, NJ: Prentice-Hall.
23. G. K. AN, S. B. KIM and E. J. POWERS 1998 *Proceedings of ICASSP*, New York, 2392–2395. Optimized parametric bispectrum estimation.
24. D. R. BRILLINGER 1981 *Time Series*. San Francisco: Holden-Day Inc.; expanded edition.
25. C. L. NIKIAS and A. P. MENDEL 1993 *IEEE Signal Processing Magazine* July, 10–37. Signal processing with higher-order spectra.
26. G. H. GOLUB and C. F. VAN LOAN 1993 *Matrix Computations*. Baltimore, MD: The Johns Hopkins University Press.
27. R. A. HORN and C. R. JOHNSON 1991 *Topics in Matrix Analysis*. Cambridge: Cambridge University Press.
28. G. B. GIANNAKIS 1990 *Transactions on Automatic Control* **35**, 18–26. On the identifiability of non-Gaussian ARMA models using cumulants.
29. A. SWAMI and J. M. MENDEL 1990 *IEEE Transactions on Acoustics, Speech and Signal Processing* **38**, 1257–1264. ARMA parameter estimation using only output cumulants.
30. A. SWAMI and J. M. MENDEL 1992 *IEEE Transactions on Automatic Control* **37**, 268–273. Identifiability of the AR parameters of an ARMA process using cumulants.